

Research papers

Noble gases in shallow aquifers preserve signatures of boiling events beneath Weishan volcano of Wudalianchi volcanic field, northeast China



Shuai Wang^{a,b}, Xuelian Huang^b, Tao Wen^c, Xun Wang^{d,*}, He Wang^e, Yongjie Han^b, Zhiwei Li^f, Jian Kuang^g, Shihua Qi^{b,g,*}

^a School of Earth Resources, China University of Geosciences, Wuhan 430074, PR China

^b School of Environmental Studies, China University of Geosciences, Wuhan 430078, PR China

^c Department of Earth and Environmental Sciences, Syracuse University, Syracuse, NY 13244, United States

^d Bureau of Geology and Mineral Resources of Heilongjiang Province, Harbin 150036, PR China

^e Institute of Ecological Geology Survey and Research of Heilongjiang Province, Harbin 150030, PR China

^f Science and Technology on Reliability and Environmental Engineering Laboratory, Beijing Institute of Spacecraft Environment Engineering, Beijing 100094, PR China

^g State Key Laboratory of Biogeology and Environmental Geology, China University of Geosciences, Wuhan 430078, PR China

ARTICLE INFO

This manuscript was handled by Huaming Guo,
Editor-in-Chief

Keywords:

Wudalianchi volcanoes
Noble gases
Rayleigh distillation
Shallow aquifer

ABSTRACT

The study on whether there is a magma chamber under Wudalianchi is a hot topic recently, as it holds great significances for the theory of plate tectonics, early warning of volcano eruption and geothermal exploration. There is no near surface geothermal abnormality reported in Weishan, the widely used and well-studied tool, geochemistry of geothermal fluids and geothermal gases, cannot be applied to this area. To reveal the thermal conditions under Weishan, we conducted a study about the abundances and isotope ratios of dissolved noble gases in shallow groundwater and springs of Weishan. The concentrations of noble gases display obvious Ne excesses and mass-dependent differentiation, the isotopic ratios indicate that Ne, Ar, Kr, and Xe are atmosphere-derived noble gases (ANGs). We apply the closed-system equilibrium (CE) model to process the data of noble gases, and indicate that the excess ANGs are not caused by the increased hydrostatic pressure or diffusive influx. Neither meltwater mixing nor oxygen consumption alone could generate sufficient noble gas excesses in our samples. Based on the reconstructed abundances of noble gases in vapor phases produced at different boiling temperatures, which are calculated according to the boiling model established on Henry's law, we conclude that the abundances of noble gases in these samples were influenced by vapor-liquid partition caused by underground boiling. The diagrams of $^{84}\text{Kr}/^{36}\text{Ar}$, $^{20}\text{Ne}/^{36}\text{Ar}$ and $^{130}\text{Xe}/^{36}\text{Ar}$ confine the temperature range where the boiling events occur in $\sim 100\text{ }^{\circ}\text{C}$ - $300\text{ }^{\circ}\text{C}$. We argued that the excess ANGs in shallow groundwater are geochemical evidence of boiling events, which seems to be continuously happening during the time range confined by the young groundwater in basalt aquifer and old groundwater in sandstone aquifer. Our findings also corroborate the recent results of geophysical survey works that a potential magma chamber exists under Weishan area. We suggest that noble gases dissolved in shallow aquifers represent a reliable geochemical tool to unveil subsurface geothermal state, where no near-surface thermal anomaly occurs.

1. Introduction

Most of the world's volcanoes occur at plate boundaries (Morgan, 1968). Located 1600 km away from the Japan arc (Fig. 1a), Wudalianchi is a typical intraplate volcanic field (Zhao, 2007) on continent, which makes Wudalianchi a special case to the theory of plate tectonics. Fig. 1b shows the subducting profile of the west Pacific plate, and similar to Changbaishan volcano, which is the largest active volcano in northeast

China, Wudalianchi volcanism is driven by the dehydration of stagnant part of subducting Pacific slab (Huang and Zhao, 2006; Zhao, 2007; Zhang et al., 2018; Zhao, 2021). Surface wave tomography of NE China indicates an occurrence of mantle upwelling beneath Wudalianchi (Ma et al., 2018; Lu et al., 2020), and this phenomenon could be related to mantle upwelling beneath Changbaishan through a secondary mantle convection (Guo et al., 2016; Zhao, 2021). According to the geochemical analyses of potassic basalt samples, the magma temperature of the

* Corresponding authors at: School of Environmental Studies, China University of Geosciences, Wuhan 430078, PR China (S. Qi).

E-mail addresses: 3376763711@qq.com (X. Wang), shihuaqi@cug.edu.cn (S. Qi).

1719–1721 CE eruption is estimated to be ~ 1250 °C (Kuritani et al., 2013), which indicates that the magmas supply for Wudalianchi volcanic eruptions are primarily derived from the asthenospheric mantle. The C-He isotopic compositions of bubbling gases in cold springs of Wudalianchi (see Fig. 1c) have been well studied (Jianguo et al., 1999; Xu et al., 2013; Mao et al., 2018; Zhao et al., 2019), and the $^3\text{He}/^4\text{He}$ ratios, ranging from 1.88 Ra to 3.87 Ra with an average value of 3.0 ± 0.4 Ra (Zhao et al., 2019), clearly indicate a presence of mantle component (Mao et al., 2009; Zhao et al., 2019). $\delta^{13}\text{C}$ values of CO_2 range from -8.8 ‰ to -3.1 ‰ , consistent with the $\delta^{13}\text{C}_{\text{CO}_2}$ values of island arc volcanic gases, which range from -9.1 ‰ to -1.3 ‰ (Sano and Marty, 1995). These studies about C-He isotopic compositions manifest the occurrence of a mantle component released and transferred to the surface of Wudalianchi by Cenozoic extension-related magmatic activities.

The multitude of needs for the research on plate tectonics, early warning of volcanic eruption hazards, and geothermal exploration warrant the discussion of whether the magma chamber under Wudalianchi exists. Recent regional geophysical survey works found a potential magma chamber beneath Weishan volcano of Wudalianchi volcano field. Based on dense array seismic imaging, Li et al. (2016) found low-velocity bodies beneath the Weishan volcano of Wudalianchi,

and these low-velocity anomalies are interpreted as manifestation of a magma chamber at a depth of ~ 7 – 13 km with an estimated volume of 200 km^3 . 3-D magnetotelluric imaging work illuminates the high-resolution spatial distribution of a very low-resistivity body at a depth of ~ 8 – 15 km beneath the Weishan volcano, it reconfirms that there exists a magma chamber (Gao et al., 2020). The eruption sequence of Wudalianchi volcanoes corroborates the existence of an uncooled magma chamber under Weishan. However, there is no near surface geothermal abnormality to indicate the existence of magma chamber beneath Weishan, and the lack of geothermal fluids and geothermal gases makes it an urgent task to seek suitable geochemical tools that can verify the above-mentioned geophysical results.

The two prominent properties of noble gases (He, Ne, Ar, Kr, and Xe), inertness and rareness, make noble gases excellent tools for tracing the source, migration, and mixing of subsurface fluids (Hilton and Craig, 1989; Ballentine et al., 2005; Castro et al., 2009; Kendrick et al., 2011; Crossey et al., 2016). In particular, isotopic ratios of He and Ne are well-established tracers for mantle gas/fluid provenance. Fractionated atmosphere-derived noble gases (ANGs) signatures have been proved to be a robust tool to document thermal events (Mazor, 1977; Wen et al., 2018; Byrne et al., 2021). Ma et al. (2009) and Warrier et al. (2013)

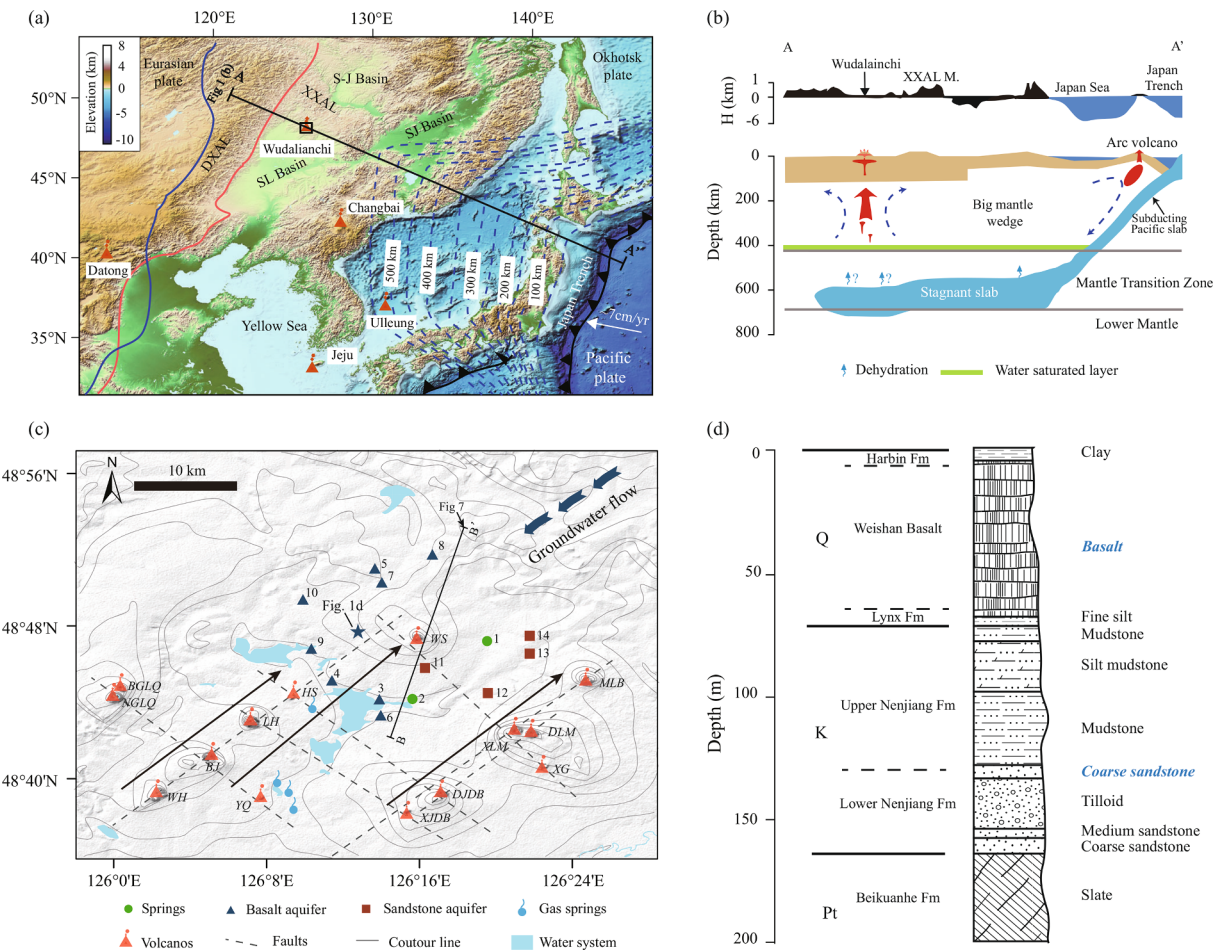


Fig. 1. Schematic map showing (a) Location of Wudalianchi within the continental intraplate setting. Black dashed lines indicate depth contours of the upper boundary of subducting Pacific slab, after Liu et al. (2017). The blue lines denote the topographic boundary, and the red curved lines denote the western edge of the stagnant Pacific slab in the mantle transition zone, after Huang and Zhao (2016). The black rectangular in Fig. 1a shows the location of Fig. 1c. DXAL, Daxinganling Mountain; XXAL, Xiaoxinganling Mountain; S-J Basin, Sunwu-Jiayin Basin; SJ Basin, Sanjiang Basin; SL Basin, Songliao Basin. (b) A-A' profile in Fig. 1a showing the subduction of the west Pacific plate, after Zhao, (2021). (c) Distribution of the sampling locations. Black arrows indicate the eruption sequence of these volcanoes. WS, Weishan; HS, Huoshaoshan; LH, Laoheishan; BJ, Bijiashan; WH, Wohushan; BGLQ, Beigelaqiushan; NGLQ, Nangelaqiushan; YQ, Yaoquanshan; MLB, Molabushan; DLM, Donglongmenshan; XLM, Xilongmenshan; XG, Xiaogushan; DJDB, Dongjiaodebushan; XJDB, Xijiaodebushan. (d) Stratigraphic succession of Weishan. Units for which formation (Fm) groundwaters were sampled in this study are marked by blue italics. (For interpretation of the references to colour in this figure legend, the reader is referred to the web version of this article.)

report the dissipation of noble gases in deep brines in the Michigan Basin, those escaping noble gases from the brine be captured and recognized by the shallow groundwater, resulting in moderate (~20–60 % Ne excess) and large (~80–>120 % Ne excess) excess of noble gases in the shallow groundwater relative to air saturated water (ASW).

Previous research of noble gases as indicators for thermal events mainly took geothermal water, geothermal vapor, natural gases (e.g. Pinti et al., 2017; Harðardóttir et al., 2018; Wen et al., 2018; Marty et al., 2020; Byrne et al., 2021), or deep brines (Ma et al., 2009) as study materials. Here, we collected groundwater samples from shallow aquifers in the vicinity area of Weishan volcano of Wudalianchi and analyzed them for the abundances and isotopic ratios of dissolved noble gases. We strive to take Weishan as a natural laboratory for studying whether the shallow groundwater could capture and preserve the signature of deep thermal abnormality. Noble gas abundances of our samples display a clearly mass-dependent fractionation pattern contrasting with that of ASW, which, after ruling out other possible causes (i.e., hydraulic pressure related mechanisms and the influence of other external factors), is identified as a result of vapor–liquid phase separation after boiling events. The combined analysis of ^{20}Ne , ^{36}Ar , ^{84}Kr , and ^{130}Xe in ANGs further indicates that the temperatures of these boiling events range from 100 to 300 °C. This study provides geochemical evidence for a potential magma chamber beneath the Weishan volcano of the Wudalianchi intraplate volcanic field, and also pioneers the utilization of dissolved noble gases in shallow aquifers to investigate deep subsurface geothermal behavior for regions where no near-surface thermal abnormality occurs.

2. Geological and hydrogeological background

Located at the transition zone between the Xiaoxinganling Mountain (denoted as “XXAL”) and the Songliao Basin (SL Basin; Fig. 1a), Wudalianchi volcano field (WDF) is one of the widely distributed Cenozoic volcanic fields surrounding the Songliao Basin. According to the recent high-resolution P-wave tomography works carried out by Wei et al. (2019) and Lu et al. (2020), a hot and wet upwelling flow was revealed in the crust and big mantle wedge under WDF, which indicates an association between the formation of the Wudalianchi volcanoes and the upwelling of asthenospheric materials above the stagnant part of Pacific slab that subducted into the mantle transition zone (Fig. 1b). A series of 14 Cenozoic volcanoes (Fig. 1c) with eruption period from ca. 2.5 Ma to ca. 0.3 ka are located in the northernmost of WDF, among which Weishan volcano erupted at about ca. 50 ka (Gao et al., 2020). Two developed faults intersect these Wudalianchi volcanoes with a main fault striking NNE and the other striking NW (Fig. 1c). In general, the 14 volcanoes erupted in sequence from southwest to northeast (Fig. 1c), indicating the potential existence of new or residual magma chamber under Weishan volcano.

WDF is generally covered by Quaternary unconsolidated sediment, and the pre-Quaternary strata are scattered, which is very conducive to the infiltration and replenishment of atmospheric precipitation. XXAL in the north of WDF is the recharge area of WDF’s groundwater. The overall groundwater flow direction in the WDF is from northeast to southwest (Wang et al., 2021). Located in the middle temperate continental seasonal climate zone, WDF holds an annual average temperature of 0.5 °C as estimated from the Wudalianchi City Meteorological Observatory data from 1980 to 2019. The lowest monthly temperature appears in January, and the average monthly temperature of January from 1980 to 2019 is -24 °C. The highest monthly temperature appears in July, and the average monthly temperature of July from 1980 to 2019 is 21.1 °C. The multi-year average precipitation is 514.3 mm, and the wet season spans from June to August.

Basalts are exposed on the surface of Weishan area. Late Cretaceous Nenjiang Formation mudstone, silt mudstone, argillaceous siltstone and gravel-bearing mudstone underlie the Quaternary strata. The underlying rocks are schist, quartzite, slate and phyllite of Beikuanhe Formation

from Neoproterozoic to Early Cambrian, more details are shown in Fig. 1d. Two main shallow aquifers are developed in Weishan area: Quaternary basalt phreatic aquifer and Cretaceous sandstone confined aquifer. In the phreatic aquifer, pores and fractures are developed in basalts. The water table depth is 10–50 m with the hydraulic head ranging from 2 to 5 m. Unlike hydraulic head, the aquifer thickness varies greatly with an average of 6 m. As for the confined aquifer, the thickness of this aquifer varies from 5 to 30 m, and the depth of the top of the confined aquifer is about 100–120 m. The hydraulic head in the confined aquifer declines from 31 m to 1 m along with the water flow.

3. Samples and methods

In this study, 2 spring samples and 12 well water samples were collected, including 8 phreatic aquifer samples from basalt layer and 4 confined aquifer samples from coarse sandstone layer. Sample locations are shown in Fig. 1c. When collecting groundwater samples from well, we first pumped the wells for ~1 h before allowing the water to flow through the 40 cm, 3/8" long, refrigerated copper tube (~14 cm³) via a stainless steel hose. After the pH and temperature of the water stabilize, both ends of the copper tube are clamped after checking air bubbles. As for spring samples, a small peristaltic pump was used to pump water through a plastic hose into copper tube, and the plastic hose was placed as close to the mouth of the spring as possible to avoid contamination.

The abundances and the isotopic ratios of dissolved noble gases (He, Ne, Ar, Kr, Xe) in the water were measured at the Natural Gas Laboratory at the University of Michigan. The analytical procedures are briefly described below, while further details can be found in Wen et al. (2016) and Wen et al. (2017). After being extracted and purified, the noble gases are captured into a computer-controlled cryogenic separator at about 10 K. Then with the temperature in cryogenic separator increasing, He, Ne, Ar, Kr and Xe are sequentially released from the cryogenic separator at 42, 80, 205, 215, and 280 K and introduced into the mass spectrometer. He and Ne were transferred into the Thermo Scientific® Helix SFT mass spectrometer, while Ar, Kr and Xe were introduced into the ARGUS VI mass spectrometer. The standard errors for He, Ne, Ar, Kr, and Xe concentration were 1.5 %, 1.3 %, 1.3 %, 1.5 %, and 2.2 %, respectively.

4. Results

Sample types, well depths, noble gas abundances and noble gas isotopic ratios are listed in Table S1 and Table S2 (Supplementary materials). Noble gas concentrations of ASW under local annual modern recharge conditions (0.5 °C, 500 m altitude) and of air are both shown for reference.

Except for samples 5 and 9, R/R_a ratios of basalt aquifer samples, where R is the measured $^3\text{He}/^4\text{He}$ ratio and R_a is the corresponding $^3\text{He}/^4\text{He}$ in air that is 1.384×10^{-6} (Clarke et al., 1976), are generally greater than 1 R_a (air value by definition) and 0.985 R_a (theoretical ASW value). In particular, R/R_a ratios of samples 4a and 4b are greater than 2 with mantle components contributing ~20 % to the terrigenic He, which is total He minus atmospheric He, in the absence tritogenic He. More detailed equations to calculate He components can be found in Ma et al. (2005). Such decoupling phenomena between mantle He and thermal manifestation have been documented before elsewhere, e.g., Wang et al. (2022) reported cold groundwater sites with R/R_a varying from 4.87 to 6.37 in Guangdong, China, and Niu et al. (2017) reported two samples of a spring site, with a water temperature of 15.3 °C, in the Island of Maui, Hawaii, and the R/R_a values are 3.82 and 4.27, respectively. R/R_a ratios of samples from sandstone aquifer are less than 1, but higher than the typical crustal R/R_a range, which is 0.02–0.05 (Oxburgh et al., 1986). If mantle components were mixed into the basalt aquifer with the deep groundwater through faults, it is hard to avoid mixing such groundwater into the sandstone aquifer, which is underneath the basalt aquifer, indicating that except for atmospheric components, there are also

mantle components mixed into the groundwater of sandstone aquifer to make the R/R_a values higher than typical crustal values. R/R_a values for our spring samples are close to 1, indicating atmospheric origin. Unlike He isotopic ratios, Ne, Ar, Kr and Xe isotopic ratios of our samples generally present atmospheric values within $\pm 1\sigma$ errors (Table S2, Supplementary materials), indicating an apparent decoupling behavior of He and other noble gas isotopes.

Fig. 2a displays total measured abundances for each noble gas element normalized to ASW values under local modern recharge conditions. With respect to ASW, all samples present He excesses (Fig. 2a), which are mainly composed of atmospheric, crustal and mantle components. Except for sample 12a, all samples show Ne excesses that are calculated by $(C_{Ne} - C_{ASW})/C_{ASW}$, which vary from 4.6 % to 549.4 %, and the samples of basalt aquifer display higher Ne excesses than that of samples from springs and sandstone aquifer. To highlight the abundance pattern of ANGs, Fig. 2b displays the same normalized data except for He, which holds excess mantle and crustal components besides atmospheric components, samples 5, 7 and 9, whose trends are displayed distinctly in Fig. 2a, are also excluded from Fig. 2b for visual purpose. We illustrate the samples by sample type in Fig. 2b, these three subsets show different levels of Ne excesses: samples from sandstone aquifer display moderate Ne excess varying between 4.6 % and 30.1 %, while samples from basalt aquifer show high Ne excesses varying between 11.1 % and 549.4 %, and 2 spring samples display slightly Ne excesses (5.1 % for sample 1 and 4.7 % for sample 2).

An overall mass-dependent pattern, that the heavier noble gases are more depleted than the lighter ones, is displayed in Fig. 2b, and most samples display an excess of Ne and a depletion of Kr and Xe compared with ASW values. A similar mass-dependent pattern was previously observed in groundwater of Hawaii (Niu et al., 2017), and suggested to be related to weather patterns, e.g., cloud heights and rainfall amount. For our samples, however, weather pattern failed to explain the extremely high atmospheric Ne excesses, thus we list other possible reasons in section 5.1, then discuss their possibilities.

5. Discussion

5.1. ANG excesses —hydrostatic pressure influence or external factors

The concentration of noble gases in ASW is a simple function of the

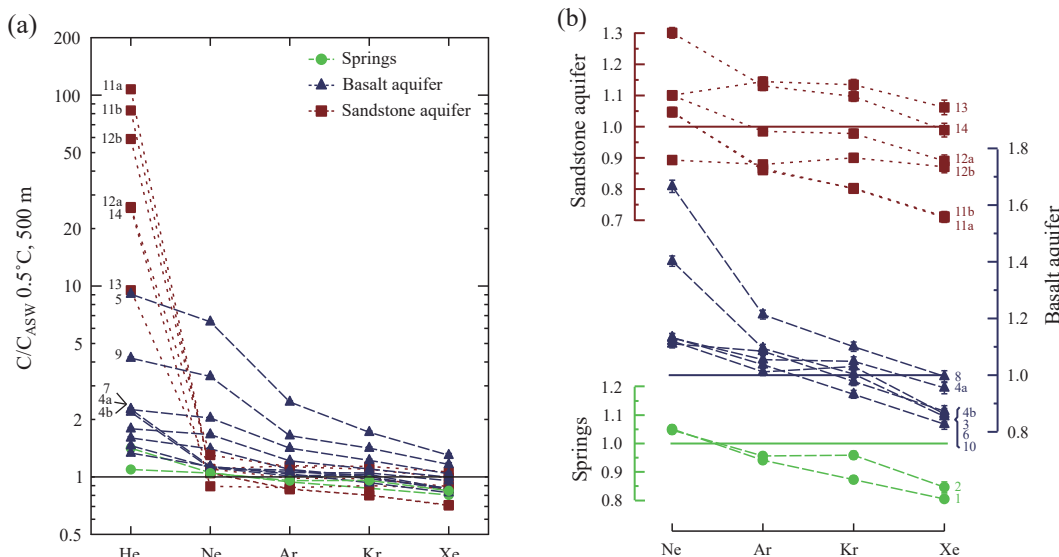


Fig. 2. (a) Total measured noble gas concentrations normalized to ASW with temperature 0.5 °C and altitude 500 m. The solid black line indicates noble gas concentrations with no addition or loss of noble gases compared to ASW. (b) Measured noble gas concentrations (without He) normalized to ASW with separated vertical axes for samples from sandstone aquifer, basalt aquifer and springs. For visual purposes, samples from sites 5, 7, and 9 are removed as they show high ANG excesses, which make the fractionation trend between light and heavy noble gas elements obvious in panel a. The symbols are same with the panel a.

temperature and pressure near the water table when groundwater is recharged. In addition to the temperature-related ASW component, groundwater also contains excess air, which is caused by the fluctuation of groundwater table. The parameters derived from the CE model hold clear physical meanings (Grundl et al., 2013; Klump et al., 2008; Markovich et al., 2020; Warrier et al., 2013), and have been widely used to discuss the formation of excess air in groundwater (Aeschbach-Hertig et al., 2002; Grundl et al., 2013; Kipfer et al., 2002; Klump et al., 2008; Markovich et al., 2020; Severinghaus and Battle, 2006; Warrier et al., 2013). Through analyzing the parameters calculated by the CE model, the cause of excess ANGs in groundwater can be identified, i.e., hydraulic pressure driven excess air dissolution or mostly controlled by the addition of external gases other than excess air. According to the CE model output, Klump et al. (2008) found that the excess ANGs in the sedimentary aquifer in southeastern Wisconsin are due to the change of hydrostatic pressure caused by the growth of ice covers. Warrier et al. (2013) found that the large excess ANGs in the Michigan Basin are not caused by the increased hydrostatic pressure, but by external additions outside the aquifer.

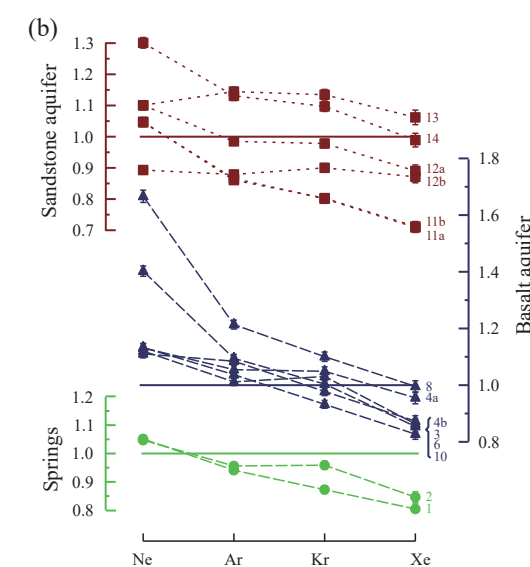
The concentrations of dissolved noble gases in water (C_{iw}) are described as.

$$C_{iw} = C_{iw}^{eq} \left(1 + \frac{(1-f)VH_i}{1+fVH_i} \right) \quad (1)$$

where the index i refers to any noble gas species, C_{iw}^{eq} is the ASW component, V is the volume of trapped air in per unit volume of water, H_i is Henry's constant for noble gas i , and factor f refers to the fractionation factor established for describing the volume variation of trapped gas as a result of bubble dissolution. The value of f usually varies from 0 to 1, represents different dissolution degrees of trapped gas, where $f = 0$ means that all trapped air bubbles are dissolved completely, $f = 1$ indicates that the samples have no bubbles dissolution and f greater than 1 indicates that water sample is degassing ((Aeschbach-Hertig et al., 2008; Warrier et al., 2013)). f can be calculated by

$$f = \frac{v}{q} \text{ with } v = \frac{\sum_i n_b}{\sum_i n_a} \text{ and } q = \frac{P_b - e}{P_a - e} \quad (2)$$

where v is the ratio of trapped air volumes in the final and initial states of dissolution respectively, q is the ratio of the dry gas pressure in the



trapped air to that in free atmosphere, n refers to the volume of noble gas i in air bubble, P is dry gas pressure of the trapped air, and e is the vapor pressure of saturation water. Subscripts a and b represent the air bubbles states in the initial and final dissolution, respectively.

Different from the Ne excess ratios used above, which are compared with Ne abundances in ASW with temperature of 0.5 °C and altitude of 500 m, we utilize the processed outputs of CE model δNe values in this section to discuss atmospheric noble gas excesses (see in Fig. 3 and Table S3). All of our samples from springs, basalt aquifer and sandstone aquifer show high amounts of δNe values ($\delta\text{Ne} = 10.0\text{--}85.01\%$), with some samples (sample 5, 7 and 9) are even higher than the typical values of δNe in groundwater ($\delta\text{Ne} = \sim 10\text{--}50\%$; see Kipfer et al. (2002)). Air contamination during sample collecting could lead to atmospheric Ne excesses, but failed to explain the fractionation between light and heavy noble gas elements, as the elemental composition of noble gases in dry air (Ozima and Podosek, 2002) is not mass-dependent. Thus, we need

other mechanisms instead of air contamination to explain the regional systematic Ne excesses.

In continental aquifer systems, δNe values of $> \sim 80\%$ have rarely been reported. Two main mechanisms were previously suggested to explain the abnormally high δNe in groundwater: hydraulic pressure related mechanisms and the influence of external factors. The hydraulic pressure related mechanisms contain (1) more frequent intense rain events, (2) the advancing of ice covers (Klump et al., 2008), and (3) enhanced fluctuations of groundwater table (Beyerle et al., 2003; Kulongoski et al., 2009). The external factors include: (1) admixture of glacial meltwater (Niu et al., 2015), and such meltwater is reported to contain as high as hundreds of percent of δNe (Loose et al., 2009), (2) the diffusive influx of excess air from the deep, and (3) the O₂ depletion without the corresponding increase of CO₂, will lead to an increase in the noble gases partial pressure in the unsaturated region (Hall et al., 2005), and (4) the addition of released ANGs from the past boiling event at depth, which subsequently were transported to shallow aquifers along with groundwater convection (Ma et al., 2009; Warrier et al., 2013).

Fig. 3a shows the calculated fractionation factor f as a function of Ne excess derived from the CE model. The best-fitting lines for sandstone aquifer samples and basalt aquifer samples are made individually. The f values of basalt aquifer samples range from 0 to 0.89 and δNe values range from 10.00 % to 85.01 %. The f values of sandstone aquifer samples range from 0 to 0.90 and δNe values range from 10.00 % to 24.73 %. The f values of sample 10 in the basalt aquifer and sample 12a in the sandstone aquifer are 0, indicating that the trapped noble gases were completely dissolved. The f values of the other samples (including spring samples) range from 0 to 1, indicating that the entrapped noble gas was dissolved with different degrees. The correlations between f and δNe of samples from basalt aquifer and sandstone aquifer are negative, both with $R^2 = 0.98$, respectively. The negative correlations between f and δNe suggest that the large amount of dissolved excess air is due to more thorough dissolution (low f value indicates high dissolution level) of the captured bubbles, in other words, lower f fractionation level. So the increase in Ne excess of our samples is controlled by dissolution instead of diffusive influx, which will further be consolidated by the discussion about isotope fractionation conditions in section 5.2.2.

The fitting line between q and δNe is approximately horizontal for samples from sandstone aquifer (Fig. 3b), the δNe values of our samples from sandstone aquifer range from 10.00 to 24.73 (Table S3), while q values that represent hydrostatic pressure are not significantly changed (vary from 1.00 to 1.05), indicating that the large amount of ANG excesses in the sandstone aquifer is unrelated to the increase of q , which emphasized the possibility of external factors. The calculated f , v , and q values of spring samples are similar with that of samples from sandstone aquifer, so in the absence of sufficient data to fit, we can assume that the ANG excesses in springs are also not related to q . Different from samples from sandstone aquifer, the q values among the samples from basalt aquifer, which vary from 1.00 to 3.88, display a larger range of variation, but the correlation between their q and δNe is not strong enough to exclude the influence of external factors ($R^2 = 0.77$). Different from the condition of sandstone layer, ANGs excesses in basalt aquifer seem to be caused by the joint influence of hydrostatic pressure increase and external factors.

According to Eq (2), both q and volume ratio v of trapped bubbles affect the solubility of bubbles, and the increase of hydrostatic pressure (high q value) will lead to the increase of noble gases solubility in groundwater, which in turn will reduce the gas volume ratio v . δNe of our samples is negatively correlated with f but has no correlation with q , this suggest a negative correlation between δNe and v , which is verified by the strong negative between v and δNe shown in Fig. 3c, with $R^2 = 0.99$ for samples from sandstone aquifer and $R^2 = 0.93$ for samples from basalt aquifer, and such strong negative correlations suggests that the increase of excess air dissolution is due to the decrease of trapped gas volume ratio v without significant influence of hydrostatic pressure increase. Therefore, we propose that external factors contribute to the

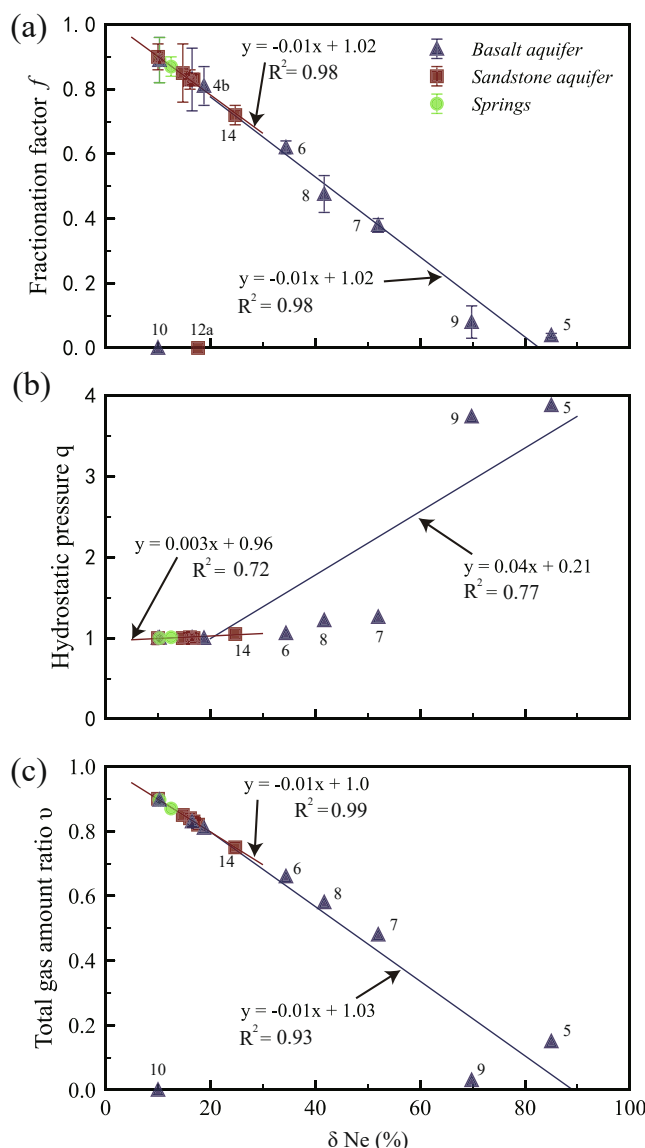


Fig. 3. Comparison of CE model derived parameters (Fractionation factor f , hydrostatic pressure q and total gas amount ratio v) with the amount of Ne excess (δNe) for Weishan samples. Best-fitting lines and coefficient of determination R^2 for samples from sandstone layer, and samples from basalt layer are given separately (black line for basalt samples and russet lines for sandstone samples). Samples 10 and 12a are excluded for fitting calculation as they show a large deviation from the normal range.

large amounts of excess ANGs in Weishan area, which we will further discuss below.

We found no evidence of pure glacial meltwater infiltration, as there was no exceptionally large δNe content on the order of glacial meltwater (several hundred percent of excess Ne) in our samples. Additionally, according to the groundwater isotopes analysis carried out by Wang et al. (2021), D and ^{18}O isotopes of Weishan groundwater display no strongly depletion, and local hydrogeologic condition indicates that groundwater recharge of WDF is driven largely by atmospheric precipitation, thus we can rule out the possibility that glacial meltwater were added to the groundwater. According to the calculation by Warrier et al. (2013), the maximum excesses of noble gases produced by an oxygen depletion (OD) mechanism without the corresponding increase of CO_2 is only $\sim 26.6\%$. The δNe values of our samples from basalt aquifer ($34.4 \sim 85.01\%$) are much higher than $\sim 26.6\%$. Therefore, the contribution of OD mechanism, if any, to the Ne excess of our water samples, will be minor or even negligible.

To further investigate the possibility of other external factors, we evaluate the enrichment or depletion degree of noble gases relative to air composition by introducing the factor $F(i)$ (Wen et al., 2018), which can be used to evaluate whether boiling or condensation signal occurs in the origin reservoir of the samples. $F(i)$ is calculated by normalizing the volume fractions of measured noble gas isotope (i) to the corresponding noble gas isotope value in air, while ^{36}Ar is taken as the reference isotope, i.e. $F(i) = (i/^{36}\text{Ar})_{\text{measured}} / (i/^{36}\text{Ar})_{\text{air}}$.

Fig. 4a and 4b respectively illustrate the measured R/R_a values compared to $F(^{20}\text{Ne})$ and $F(^{130}\text{Xe})$ values. Most of the samples show deviations to different degrees from the ASW values (Fig. 4), which can be explained by mixing the ASW with other end members, including atmospheric (air), mantle, crustal, and boiling vapor phase of atmospheric noble gases. In both Fig. 4a and 4b, samples 5 and 9 show an offset towards air end member, indicating the addition of air or fractionated vapor phase originated from pure ASW without crustal or mantle components.

In Fig. 4a, samples 13 and 14 indicate the mixing between ASW and ASWC (ASW with the addition of crustal Helium), while in Fig. 4b, a slight contribution of vapor phase fractionation is observed in samples 13 and 14. The rest samples display a mixing trend between ASW and ASWM (ASW adding mantle Helium), and both in Fig. 4a and 4b, trends of vapor phase fractionation occur. These mixing trends consolidate the hypothesis that the element fractionation among heavy and light noble gases observed in shallow groundwater as well as springs in Weishan area is a result of mixing with vapor phase, which is the product of vapor–liquid separation caused by potential boiling events under Weishan. Although there is no near-surface geothermal abnormality

displayed near Weishan area, recent geophysical results, which display low-velocity anomaly (see A-A' and B-B' cross sections of shear wave velocity from Li et al. (2016)) and low-resistivity body (see all four cross sections of resistivity from Gao et al. (2020)) at the depth of ~ 10 km in the crust of Weishan that are interpreted as a potential magma chamber, reinforce our speculation of modern underground boiling events under Weishan.

After ruling out all the possible external factors described in section 5.1 except for boiling events, we argue that the atmospheric Ne excesses observed in Weishan area are ANG remnants released from the boiling of the deep fluids to the shallow layer.

5.2. Noble gas pattern as implication for thermal event under Weishan volcano

Noble gas signals of vapor phase from vapor-liquid fractionation have been reported in several hydrothermal systems, such as the Los Azufres geothermal field in Mexico (Wen et al., 2018) and the Icelandic geothermal system (Byrne et al., 2021). Noble gas signals in residual liquid phases have also been reported, such as brines that show noble gas depletion in deep aquifer of the Michigan Basin (Ma et al., 2009). In order to further evaluate the likelihood of the underground boiling events and the temperature at which the boiling occurred and vapor phase be separated, we adopted a boiling model established on Henry's Law to reconstruct the abundances of vapor phase noble gases for different temperatures, and compared them with our data for interpretation.

5.2.1. The boiling model

According to Henry's Law, Mazor and Truesdell (1984) established the boiling model to describe the fractionation degree of noble gases between vapor and liquid phases. When a boiling event occurs, a mass balance can be used to describe the fractionation of a noble gas from initial ASW into vapor phase and residual liquid phase:

$$C_{\text{asw}} = X_v C_v + (1 - X_v) C_l \quad (3)$$

where C_{asw} , C_v and C_l are the noble gas abundances (e.g., ^{20}Ne , ^{36}Ar , ^{130}Xe) dissolved in the initial ASW, vapor phase (steam) and residual liquid respectively, X_v and $1 - X_v$ represent the fractions of vapor phase and residual liquid phase after boiling occurs respectively.

A is the fractionation coefficient of noble gases between liquid phase and vapor phase, can be calculated by:

$$A = \frac{C_v}{C_l} \quad (4)$$

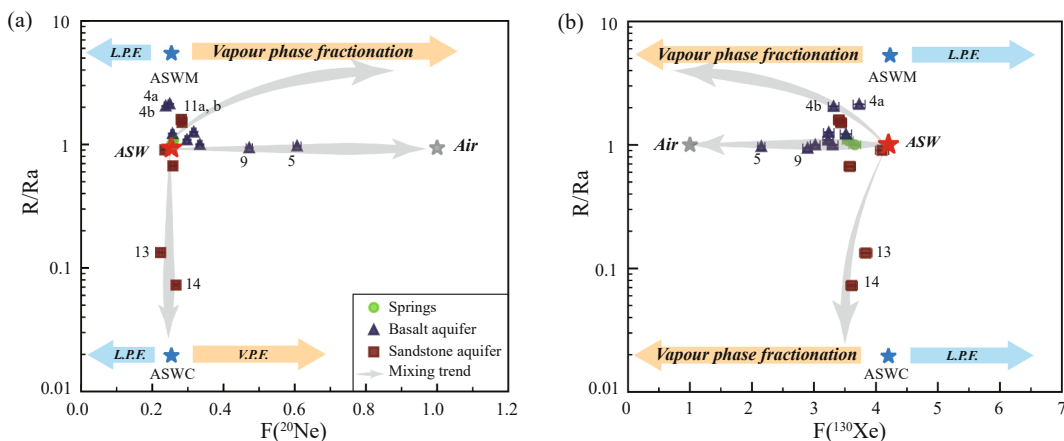


Fig. 4. (a) $F(^{20}\text{Ne})$ ratios and (a) $F(^{130}\text{Xe})$ ratios plotted vs the helium isotopic compositions not corrected for air contamination (R/R_a). L.P.F. is short for liquid phase fractionation and V.P.F. is short for vapor phase fractionation. The isotopic variations of helium and elemental abundances of atmospheric noble gases can be explained by vapor phase mixing into ASW in shallow aquifers. Air addition in two of our samples (samples 5 and 9) is likely due to air contamination.

By substituting Eq. (4) into Eq. (3), a formula can be derived to calculate the noble gas abundance in vapor phase as a function of X_v and A.

$$C_v = \frac{AC_{\text{asw}}}{(A-1)X_v + 1} \quad (5)$$

The coefficient A is temperature-dependent, and can be calculated for each noble gas at a given temperature (Wagner and Pruss, 1993; Harvey, 1996; Ozima and Podosek, 2002; Fernández-Prini et al., 2003; Byrne et al., 2021), the calculating methods and needed parameters are outlined in supplemental text.

5.2.2. Noble gas abundances indicate boiling events

When evaluating the noble gas differentiation, the highest atmosphere-derived isotope abundance for each element is usually considered (^{20}Ne , ^{36}Ar , ^{84}Kr , ^{130}Xe , and ^{132}Xe can be used when fissionogenic Xe is negligible) (Byrne et al., 2021). Using Eq. (5), we can calculate the maximum fractionation of vapor phase, which occurs at the initial partitioning ($X_v = 0$). Fig. 5 illustrates the maximum fractionation vapor phase line that fractionated from the initial ASW phase in a certain temperature range, and except for samples 5 and 9 that offset towards air end member, noble gas abundances of our samples are close to the vapor phase fractional line, showing that ^{20}Ne , ^{36}Ar , ^{84}Kr , ^{130}Xe abundances are in good correlation with boiling temperature, which consolidates our speculation that external factors influence noble gas

pattern in Weishan area, and the external factor for our samples refer to the addition of vapor phase caused by boiling events.

It should be noted that, as shown in Fig. 5, mixing with ASW will move data points toward the ASW end member, resulting in overestimated temperature records. In addition, continuous fractionation will also reduce the abundance of noble gases, leading to data points moving downwards along the vapor phase line, which will also lead to overestimated temperature records. The temperature range in Fig. 5, where our samples are located, is not the real boiling temperature range, which requires other analytical methods to discern the influence of ASW and continuous fractionation, and we will take these factors into account when discussing about the boiling temperature range in section 5.2.3.

When there is a certain concentration gradient of noble gases in underground water, molecular diffusion is a mechanism that cannot be ignored, which can lead to the abundance differentiation among heavy and light elements of noble gases. Molecular diffusion transport is generally thought to result in mass-dependent differentiation of Ne and Ar isotopes inversely proportional to the square root relationship of their atomic mass ratios (Tyroller et al., 2014), whereas fractionation of Kr and Xe isotopes has not been observed in the molecular diffusion experiments carried out by Tyroller et al. (2018). Since the molecular diffusion coefficient of noble gases decreases with the increase of atomic mass, the diffusion rate of light noble gases (He, Ne, Ar) is much faster than that of weight noble gases (Kr, Xe), and both elements and isotopes

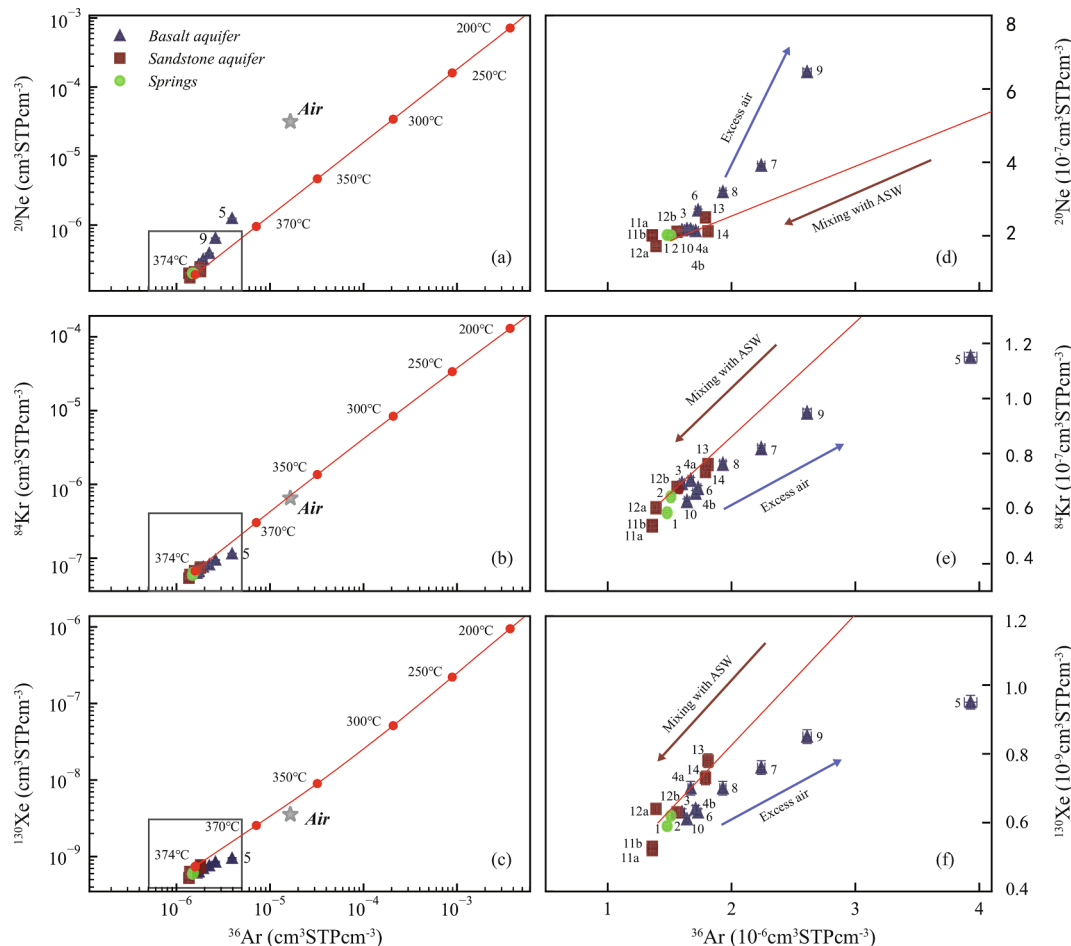


Fig. 5. Abundances of atmosphere-derived noble gas isotopes. (a) ^{20}Ne vs ^{36}Ar , (b) ^{84}Kr vs ^{36}Ar , (c) ^{130}Xe versus ^{36}Ar , (d) ^{20}Ne vs ^{36}Ar , (e) ^{84}Kr vs ^{36}Ar , (f) ^{130}Xe vs ^{36}Ar . (d-f) are Zoom-in views of the corresponding plot (a-c) in the left column. Endmember compositions of air are also shown in (a-c). Red lines represent the predicted composition of a vapour phase fractionated from an initial ASW phase over a range of temperatures, using Eq. (5) as described in the text. Selected temperatures are annotated. Except for samples 5 and 9 that offset towards Air end member, these panels show a good fit of Ne, Kr, Xe and Ar abundances to the estimated fractionation lines. (For interpretation of the references to colour in this figure legend, the reader is referred to the web version of this article.)

of light noble gases will be fractionated when diffusion occurs. If diffusion is a non-negligible factor that influences the fractionation among light and heavy noble gases of our samples, then isotope fractionations of Ne and Ar should also be observed. However, isotope ratios of Ne and Ar in our samples are very close to ASW values without significant isotopic fractionation, thus diffusive influx can be excluded as a controlling factor for noble gas pattern of Weishan, and the separated vapor after boiling should be carried into shallow aquifers by deep circulation groundwater without significant diffusion occurs.

5.2.3. Estimated temperature range at which boiling occurs

In a high enthalpy hydrothermal system with well-researched geological conditions, the required depth and temperature for the initial boiling to occur can be estimated through introducing a boiling point curve (Ma et al., 2009). When the condition of subsurface geothermal water encounters the boiling point curve, boiling event will occur as well as phase separation. In fact, the establishment of a boiling point curve is a complicated function that needs a multitude of factors, including geothermal gradient, ground stress condition and the content of dissolved gas in the fluids. However, the confirmations for every factor need more detailed information and fieldwork to support, which is beyond the scope of this research, and we will only discuss the temperature range where the boiling might occur.

According to the analysis in section 5.2.2, the concentrations of Ne, Ar, Kr and Xe are mainly controlled by temperature-dependent vapor–liquid fractionation. We can analyze the temperature range when vapor–liquid separation occurs according to the diagram based on the boiling model (Fig. 6). The maximum fractionation of this complementary vapor phase is plotted as a solid red line in Fig. 6, representing the maximum fractionation over a certain temperature range. Taking the values of X_V from 0 to 1, we can get continuous fractionation lines to show the selected annotation temperature (dashed lines in Fig. 6) according to Eq. (5).

Air addition during sampling or during degassing the samples in the laboratory will increase the ANG abundances and results in an

underestimation of the estimated boiling temperature. Samples 5 and 9 that from basalt aquifer display significantly offsets toward the air end member (Fig. 6), such air influence also can be recognized in Fig. 3b, Fig. 4 and Fig. 5, while the remaining samples are subject to negligible air influence. Samples 3, 12a and 12b are located to the right of the maximum vapor phase fractionation line, showing relative enrichment of ^{84}Kr to ^{36}Ar , which may indicate the admixture of sedimentary Kr released by organic matter (e.g., shale). High $^{84}\text{Kr}/^{36}\text{Ar}$ ratios have also been previously reported in brine samples from deep aquifer of the Michigan Basin (Ma et al., 2009) as well as in hydrocarbon-related samples from San Juan Basin (Zhou et al., 2005), and those high $^{84}\text{Kr}/^{36}\text{Ar}$ ratios have been interpreted as organic Kr release from local sedimentary matter. The fractionation between heavy and light isotopes is regionally systematic, while Kr enrichment is only shown in three samples. In this case, it can be speculated that the organic noble gases, which show Kr enrichment, are not likely to be added into the deep circulating ASW before the boiling event occurs, otherwise, our samples should display an overall ^{84}Kr enrichment accompanying the systematic mass-dependent fractionation.

As we can recognize in Fig. 6, except for samples 5 and 9 that are located above the maximum vapor phase fractionation line and samples 3, 12a and 12b that are located to the right of the maximum vapor phase fractionation line, most of the plotted data are located within the continuous fractionation lines controlled by the temperatures vary from 100 °C to 300 °C. The samples show convergence towards ASW end member, which may indicate a high degree of fractionation or/and mixing with shallow ASW. The mixing line between the ASW and the maximum fractionation point should be a straight line connecting two points, which hold no significant difference from the continuous fractionation line, so for visual purposes, the mixing lines are not drawn in Fig. 6. Due to the poor constraints at the deep conditions of Weishan area, we cannot distinguish these two possible reasons that can result in the convergence towards ASW end member, however, they both indicate the occurrence of boiling events, and they hold no significant difference under the accuracy requirements for evaluating temperature range of

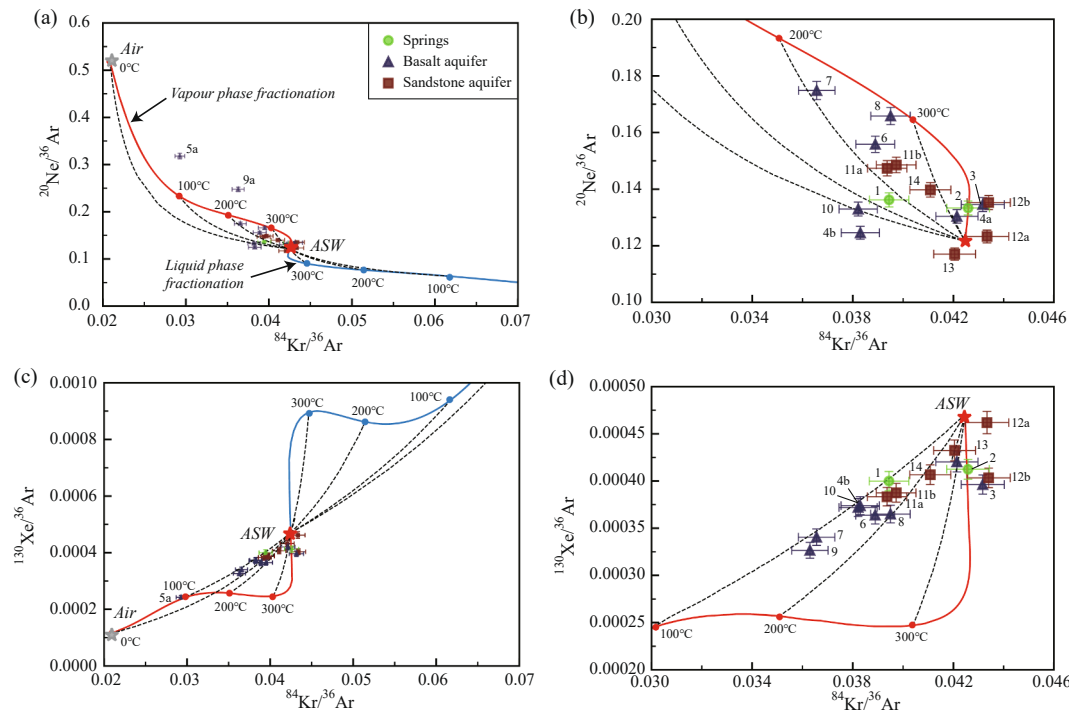


Fig. 6. Elemental ratios for noble gases, showing also expected maximum fractionation lines for the vapour phase (solid red) and liquid phase (solid blue). Dashed lines represent continued fractionation over the range $0 < X_V < 1$ for selected annotated temperatures, calculated using Eq. (5) as described in the text. (For interpretation of the references to colour in this figure legend, the reader is referred to the web version of this article.)

boiling.

If the noble gas pattern in our samples is controlled by vapor–liquid fractionation, we should expect to find samples in deeper reservoirs that can record the residual complementary liquid phase for the vapor phase signals displayed in this study, and those potential samples will locate between ASW and the maximum fractionation liquid phase line in Fig. 6. The sampling for the deeper reservoir of Weishan area will be carried out soon.

The noble gas pattern in Weishan area is caused by vapor–liquid separation due to boiling, and the separated vapor phase has undergone no obvious diffusion in the process of upward migration to shallow aquifers. We speculated that the upward migration of gas is dominated by groundwater circulation controlled by faults. Based on the above speculations, we draw a schematic plot to show the formation mechanism of the noble gas pattern of our samples (see Fig. 7). The boiling events seem to be continuously happening in the time scale confined by the time limit provided by young groundwater in basalt aquifer and old groundwater in sandstone aquifer.

According to our results (Fig. 4), high ${}^3\text{He}/{}^4\text{He}$ magma gases only affect two wells (i.e., where we collected samples 4a, 4b 11a and 11b), however, the mass related trends about element abundances of heavy noble gases (Ne, Ar, Kr and Xe) can be recognized in all of our samples (Fig. 2). This decoupling behavior between He and other noble gases indicates a different mechanism other than magmatic gases, and further discussions indicate the influence of separated vapor phase after ASW boiling. The isotopic compositions of volcanic noble gases are often indistinguishable from that of the atmosphere, that is because when volcanic gas enters the local circulation system, it is usually saturated with atmospheric noble gases that could overwhelm the mantle component except for He, which is so strongly depleted in the atmosphere. As Kaneoka (1980) pointed out, when fractionation occurs, the maximum enrichment of the ${}^3\text{He}/{}^4\text{He}$ ratio by a single mass fractionation process is not higher than 16 %. Hence, it is difficult to explain the

high ${}^3\text{He}/{}^4\text{He}$ ratios displayed in our samples by a single mass fractionation of atmospheric He, since samples 3, 4a, 4b, 8, 11a and 11b display 20 % more enrichment of the ${}^3\text{He}/{}^4\text{He}$ ratio than air value (Table S1, Supplementary materials). Meanwhile, the atmospheric characteristic of Ne and Ar isotopes seems not to support the occurrence of diffusion. Processes like diffusion and Rayleigh distillation cannot explain the high ${}^3\text{He}/{}^4\text{He}$ ratio in the sample, so it is suggested that the high ${}^3\text{He}/{}^4\text{He}$ ratios in our samples are due to inherited mantle end member characteristics. Different from the overall characteristic of atmospheric Ne excess and noble gas element fractionation in each sample, the non-atmospheric ${}^3\text{He}/{}^4\text{He}$ values only appear in a few individual samples, indicating that the additions of the crustal or mantle components have not mixed into the deep circulation groundwater before the vapor–liquid phase fractionation occurs (Fig. 7). Based on the published data we can acquire now, it's hard to distinguish the source of these mantle components, which might be from the potential magma chamber in the shallow crust under Weishan and/or from deeper reservoir.

6. Conclusions

The isotopic compositions of He in our samples show the addition of crust-derived and mantle-derived He, while the Ne-Xe isotope ratios only indicate atmospheric sources. The noble gas pattern displays a general mass-dependent trend that lighter noble gases are more abundant than heavier noble gases, and also show atmospheric Ne excesses relative to ASW under local modern recharge conditions. We have adopted the CE model to process the measured noble gas data, and the results indicate that the excess ANG in our samples is not caused by the increase of hydrostatic pressure, meanwhile, the diffusive influx is also excluded as one external factor. Through further discussion, we confirmed that there is no admixture of glacial meltwater, and oxygen depletion alone cannot generate enough noble gas excess. According to the boiling model based on Henry's Law, we reconstruct the noble gas

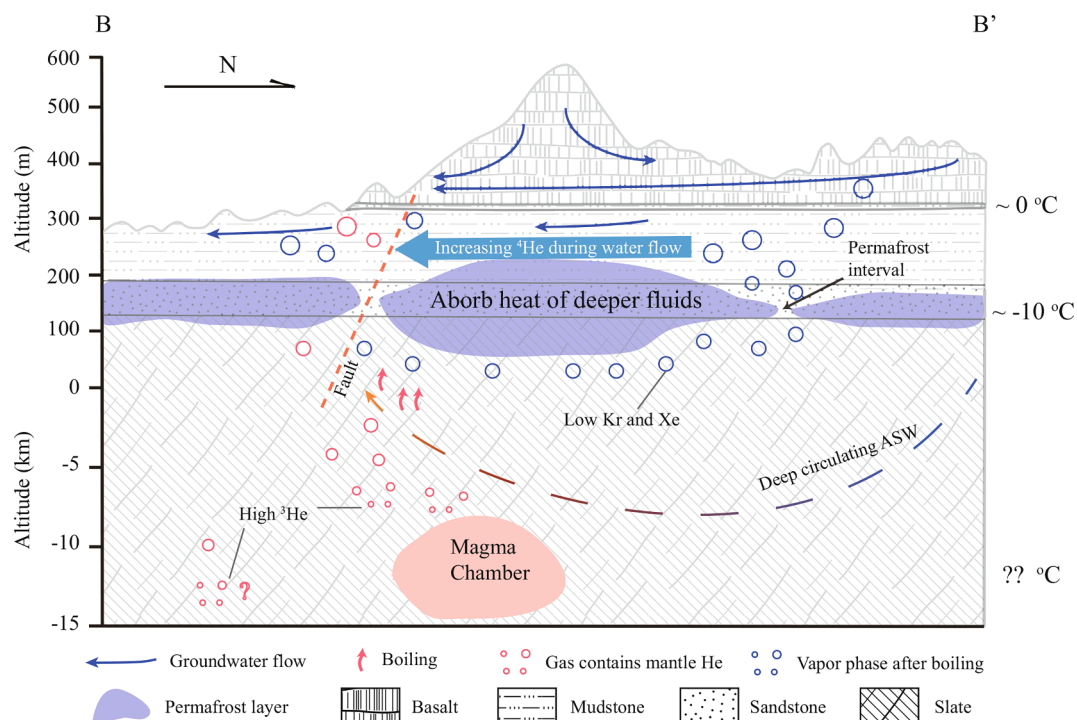


Fig. 7. Schematic of cross section B-B' in Fig. 1 (c) illustrating the formation reason of the overall Ne excess, fractionation between light and heavy noble gas elements, as well as the non-atmospheric ${}^3\text{He}/{}^4\text{He}$ values appearing in a few samples in the south of Weishan. Thickness and intervals of permafrost are not based on actual measurement but indicative. Depth range of the magma chamber is after MT work by Gao (2020). Temperatures are measured in the drilling hole of Fig. 1d. It is worth noting that the deep circulation of ASW is only a schematic path, also how the heat conduct and convect is still unclear, more detailed works are waiting to be carried out.

abundances in vapor phase of different boiling temperatures, which indicates that the abundances of ANGs in our samples are influenced by fractionated vapor phase that can be the outcome of subsurface boiling events. The results of $^{84}\text{Kr}/^{36}\text{Ar}$ vs $^{20}\text{Ne}/^{36}\text{Ar}$ and $^{130}\text{Xe}/^{36}\text{Ar}$ indicate that most of our data are located in the noble gas fractionation line from 100 °C to 300 °C, and the samples showed convergence towards the ASW end member, which can be interpreted as a high degree of fractionation or/and mixing with shallow ASW. The young groundwater in basalt aquifer and old groundwater in sandstone aquifer provides the time limit when the boiling events seem to be continuously happening. These findings strengthen the geophysical imaging results that there are potential magma chambers in the shallow crust of Weishan, which are not in equilibrium with the temperature of the surrounding rock. These incomplete cooling (hot) magmas will heat up deep circling ASW, and when the condition of hot fluids encounters the boiling point curve, boiling events will occur, generating the vapor phase that is responsible for the abnormal ANG signals in shallow groundwater of Weishan. We suggest that noble gases dissolved in shallow aquifers represent a novel geochemical tool to unveil subsurface geothermal state, where no near-surface thermal anomaly occurs.

CRediT authorship contribution statement

Shuai Wang: Conceptualization, Methodology, Writing – original draft. **Xuelian Huang:** Writing – review & editing. **Tao Wen:** Writing – review & editing. **Xun Wang:** Conceptualization, Writing – review & editing. **He Wang:** Resources. **Yongjie Han:** Writing – review & editing. **Zhiwei Li:** Methodology, Writing – review & editing. **Jian Kuang:** Writing – review & editing. **Shihua Qi:** Conceptualization, Funding acquisition, Methodology, Project administration, Resources, Supervision, Writing – review & editing.

Declaration of Competing Interest

The authors declare that they have no known competing financial interests or personal relationships that could have appeared to influence the work reported in this paper.

Data availability

The authors confirm that the data supporting the findings of this study are available within its [supplementary materials](#). Supporting data are provided in Tables S1–S3.

Acknowledgements

This study was financially supported by Institute of Ecological Geology Survey and Research of Heilongjiang Province. This study was also financially supported by the China Geological Survey (No. 1212011220014). Prof. David A. Yuen, and Zhang Hongyan gave excellent guidance in the manuscript writing, Prof M. Clara Castro, Prof Chris M. Hall and Dr Yi Niu for assisting the noble gas sampling and analyses.

Appendix A. Supplementary data

Supplementary data to this article can be found online at <https://doi.org/10.1016/j.jhydrol.2022.128246>.

References

- Aeschbach-Hertig, W., Stute, M., Clark, J.F., Reuter, R.F., Schlosser, P., 2002. A paleotemperature record derived from dissolved noble gases in groundwater of the Aquia Aquifer (Maryland, USA). *Geochim. Cosmochim. Acta* 66 (5), 797–817. [https://doi.org/10.1016/S0016-7037\(01\)00804-3](https://doi.org/10.1016/S0016-7037(01)00804-3).
- Aeschbach-Hertig, W., El-Gamal, H., Wieser, M., Palcsu, L., 2008. Modeling excess air and degassing in groundwater by equilibrium partitioning with a gas phase. *Water Resour. Res.* 44 (8) <https://doi.org/10.1029/2007wr006454>.
- Ballentine, C.J., Marty, B., Sherwood Lollar, B., Cassidy, M., 2005. Neon isotopes constrain convection and volatile origin in the Earth's mantle. *Nature* 433 (7021), 33–38. <https://doi.org/10.1038/nature03182>.
- Beyerle, U., Rueedi, J., Leuenberger, M., Aeschbach-Hertig, W., Peeters, F., Kipfer, R., Dodo, A., 2003. Evidence for periods of wetter and cooler climate in the Sahel between 6 and 40 kyr BP derived from groundwater. *Geophys. Res. Lett.* 30 (4) <https://doi.org/10.1029/2002gl016310>.
- Byrne, D.J., Broadley, M.W., Halldorsson, S.A., Ranta, E., Ricci, A., Tyne, R.L., Stefánsson, A., Ballentine, C.J., Barry, P.H., 2021. The use of noble gas isotopes to trace subsurface boiling temperatures in Icelandic geothermal systems. *Earth Planet. Sci. Lett.* 560, 116805.
- Castro, M.C., Ma, L., Hall, C.M., 2009. A primordial, solar He–Ne signature in crustal fluids of a stable continental region. *Earth Planet. Sci. Lett.* 279 (3–4), 174–184. <https://doi.org/10.1016/j.epsl.2008.12.042>.
- Clarke, W.B., Jenkins, W., Top, Z., 1976. Determination of tritium by mass spectrometric measurement of ^3He . *Internat. J. Appl. Radiat. Isotopes* 27 (9), 515–522. [https://doi.org/10.1016/0020-708X\(76\)90082-X](https://doi.org/10.1016/0020-708X(76)90082-X).
- Crossey, L.J., Karlstrom, K.E., Schmandt, B., Crow, R.R., Colman, D.R., Cron, B., Takacs-Vesbach, C.D., Dahm, C.N., Northup, D.E., Hilton, D.R., Ricketts, J.W., Lowry, A.R., 2016. Continental smokers couple mantle degassing and distinctive microbiology within continents. *Earth Planet. Sci. Lett.* 435, 22–30.
- Fernández-Prini, R., Alvarez, J.L., Harvey, A.H., 2003. Henry's constants and vapor-liquid distribution constants for gaseous solutes in H_2O and D_2O at high temperatures. *J. Phys. Chem. Ref. Data* 32 (2), 903–916. <https://doi.org/10.1063/1.1564818>.
- Gao, J.i., Zhang, H., Zhang, S., Xin, H., Li, Z., Tian, W., Bao, F., Cheng, Z., Jia, X., Fu, L., 2020. Magma recharging beneath the Weishan volcano of the intraplate Wudalianchi volcanic field, northeast China, implied from 3-D magnetotelluric imaging. *Geology* 48 (9), 913–918.
- Grundl, T., Magnusson, N., Brennwald, M.S., Kipfer, R., 2013. Mechanisms of subglacial groundwater recharge as derived from noble gas, ^{14}C , and stable isotopic data. *Earth Planet. Sci. Lett.* 369–370, 78–85. <https://doi.org/10.1016/j.epsl.2013.03.012>.
- Guo, Z., Chen, Y.J., Ning, J., Yang, Y., Afonso, J.C., Tang, Y., 2016. Seismic evidence of on-going sublithosphere upper mantle convection for intra-plate volcanism in Northeast China. *Earth Planet. Sci. Lett.* 433, 31–43.
- Hall, C.M., Castro, M.C., Lohmann, K.C., Ma, L., 2005. Noble gases and stable isotopes in a shallow aquifer in southern Michigan: Implications for noble gas paleotemperature reconstructions for cool climates. *Geophys. Res. Lett.* 32 (18), n/a–n/a.
- Harðardóttir, S., Halldórsson, S.A., Hilton, D.R., 2018. Spatial distribution of helium isotopes in Icelandic geothermal fluids and volcanic materials with implications for location, upwelling and migration of the Icelandic mantle plume. *Chem. Geol.* 480, 12–27. <https://doi.org/10.1016/j.chemgeo.2017.05.012>.
- Harvey, A.H., 1996. Semiempirical correlation for Henry's constants over large temperature ranges. *AIChE J.* 42 (5), 1491–1494. <https://doi.org/10.1002/aic.690420531>.
- Hilton, D.R., Craig, H., 1989. A helium isotope transect along the Indonesian archipelago. *Nature* 342 (6252), 906–908. <https://doi.org/10.1038/342906a0>.
- Huang, J., Zhao, D., 2006. High-resolution mantle tomography of China and surrounding regions. *J. Geophys. Res.* 111 (B9) <https://doi.org/10.1029/2005jb004066>.
- Jianguo, D., Shengqiang, L., Yi, Z., Jinzhang, R., Rubo, S., Heshun, D., 1999. Geochemical characteristics of gases from the Wudalianchi volcanic area, Northeastern China. *Acta Geol. Sinica-Engl. Ed.* 73 (2), 225–229. <https://doi.org/10.1111/j.1755-6724.1999.tb00830.x>.
- Kaneoka, I., 1980. Rare gas isotopes and mass fractionation: An indicator of gas transport into or from a magma. *Earth Planet. Sci. Lett.* 48 (2), 284–292. [https://doi.org/10.1016/0012-821X\(80\)90192-2](https://doi.org/10.1016/0012-821X(80)90192-2).
- Kendrick, M.A., Scambelluri, M., Honda, M., Phillips, D., 2011. High abundances of noble gas and chlorine delivered to the mantle by serpentinite subduction. *Nat. Geosci.* 4 (11), 807–812. <https://doi.org/10.1038/ngeo1270>.
- Kipfer, R., Aeschbach-Hertig, W., Peeters, F., Stute, M., 2002. Noble gases in lakes and ground waters. *Rev. Mineral. Geochem.* 47 (1), 615–700.
- Klump, S., Cirkpa, O.A., Surbeck, H., Kipfer, R., 2008. Experimental and numerical studies on excess-air formation in quasi-saturated porous media. *Water Resour. Res.* 44 (5) <https://doi.org/10.1029/2007WR006280>.
- Kulogoski, J.T., Hilton, D.R., Izicki, J.A., Belitz, K., 2009. Evidence for prolonged El Niño-like conditions in the Pacific during the Late Pleistocene: a 43ka noble gas record from California groundwaters. *Quat. Sci. Rev.* 28 (23–24), 2465–2473. <https://doi.org/10.1016/j.quascirev.2009.05.008>.
- Kuritanai, T., Kimura, J.-I., Ohtani, E., Miyamoto, H., Furuyama, K., 2013. Transition zone origin of potassic basalts from Wudalianchi volcano, northeast China. *Lithos* 156–159, 1–12. <https://doi.org/10.1016/j.lithos.2012.10.010>.
- Li, Z., Ni, S., Zhang, B., Bao, F., Zhang, S., Deng, Y., Yuen, D.A., 2016. Shallow magma chamber under the Wudalianchi Volcanic Field unveiled by seismic imaging with dense array. *Geophys. Res. Lett.* 43 (10), 4954–4961.
- Loose, B., Schlosser, P., Smethie, W.M., Jacobs, S., 2009. An optimized estimate of glacial melt from the Ross Ice Shelf using noble gases, stable isotopes, and CFC transient tracers. *J. Geophys. Res.* 114 (C8) <https://doi.org/10.1029/2008jc005048>.
- Lu, M., Lei, J., Zhao, D., Ai, Y., Xu, X., Zhang, G., 2020. SKS splitting measurements in NE China: new insights into the Wudalianchi intraplate volcanism and mantle dynamics. *J. Geophys. Res. Solid Earth* 125 (3). <https://doi.org/10.1029/2019jb018575>.
- Ma, L., Castro, M.C., Hall, C.M., Walter, L.M., 2005. Cross-formational flow and salinity sources inferred from a combined study of helium concentrations, isotopic ratios,

- and major elements in the Marshall aquifer, southern Michigan. *Geochem. Geophys. Geosyst.* 6 (10), n/a–n/a.
- Ma, L., Castro, M.C., Hall, C.M., 2009. Atmospheric noble gas signatures in deep Michigan Basin brines as indicators of a past thermal event. *Earth Planet. Sci. Lett.* 277 (1–2), 137–147. <https://doi.org/10.1016/j.epsl.2008.10.015>.
- Ma, J., Tian, Y., Liu, C., Zhao, D., Feng, X., Zhu, H., 2018. P-wave tomography of Northeast Asia: Constraints on the western Pacific plate subduction and mantle dynamics. *Phys. Earth Planet. Inter.* 274, 105–126.
- Mao, X., Wang, Y., Chudaev, O.V., Wang, X., 2009. Geochemical evidence of gas sources of CO₂-rich cold springs from Wudalianchi, Northeast China. *J. Earth Sci.* 20 (6), 959–970. <https://doi.org/10.1007/s12583-009-0081-5>.
- Mao, Xumei, Wang, Hua, Feng, Liang, 2018. Impact of additional dead carbon on the circulation estimation of thermal springs exposed from deep-seated faults in the Dongguan basin, southern China. *J. Volcanol. Geotherm. Res.* 361, 1–11. <https://doi.org/10.1016/j.volgeores.2018.08.002>.
- Markovich, K.H., Condon, L.E., Carroll, K.C., Purtschert, R., McIntosh, J.C., 2020. A mountain-front recharge component characterization approach combining groundwater age distributions, noble gas thermometry, and fluid and energy transport modeling. *Water Resour. Res.* 57 (1) <https://doi.org/10.1029/2020wr027743>.
- Marty, B., Almayrac, M., Barry, P.H., Bekaert, D.V., Broadley, M.W., Byrne, D.J., Ballantine, C.J., Caracausi, A., 2020. An evaluation of the C/N ratio of the mantle from natural CO₂-rich gas analysis: Geochemical and cosmochemical implications. *Earth Planet. Sci. Lett.* 551, 116574.
- Mazor, E., 1977. Geothermal tracing with atmospheric and radiogenic noble gases. *Geothermics* 5 (1), 21–36. [https://doi.org/10.1016/0375-6505\(77\)90005-0](https://doi.org/10.1016/0375-6505(77)90005-0).
- Mazor, E., Truesdell, A.H., 1984. Dynamics of a geothermal field traced by noble gases: Cerro Prieto, Mexico. *Geothermics* 13 (1), 91–102. [https://doi.org/10.1016/0375-6505\(84\)90009-9](https://doi.org/10.1016/0375-6505(84)90009-9).
- Morgan, W.J., 1968. Rises, trenches, great faults, and crustal blocks. *J. Geophys. Res.* 73 (6), 1959–1982. <https://doi.org/10.1029/JB073i006p01959>.
- Niu, Y.I., Castro, M.C., Aciego, S.M., Hall, C.M., Stevenson, E.I., Arendt, C.A., Das, S.B., 2015. Noble gas signatures in Greenland: Tracing glacial meltwater sources. *Geophys. Res. Lett.* 42 (21), 9311–9318.
- Niu, Y.I., Castro, M.C., Hall, C.M., Gingerich, S.B., Scholl, M.A., Warrier, R.B., 2017. Noble gas signatures in the Island of Maui, Hawaii: Characterizing groundwater sources in fractured systems. *Water Resour. Res.* 53 (5), 3599–3614.
- Oxburgh, E.R., O’Nions, R.K., Hill, R.I., 1986. Helium isotopes in sedimentary basins. *Nature* 324 (6098), 632–635.
- Ozima, M., Podosek, F.A., 2002. Noble gas geochemistry. Cambridge University Press.
- Pinti, D.L., Castro, M.C., Lopez-Hernandez, A., Han, G., Shouakar-Stash, O., Hall, C.M., Ramirez-Montes, M., 2017. Fluid circulation and reservoir conditions of the Los Humeros Geothermal Field (LHGF), Mexico, as revealed by a noble gas survey. *J. Volcanol. Geoth. Res.* 333–334, 104–115.
- Sano, Yuji, Marty, Bernard, 1995. Origin of carbon in fumarolic gas from island arcs. *Chem. Geol.* 119 (1), 265–274. [https://doi.org/10.1016/0009-2541\(94\)00097-R](https://doi.org/10.1016/0009-2541(94)00097-R).
- Severinghaus, J.P., Battle, M.O., 2006. Fractionation of gases in polar ice during bubble close-off: New constraints from firn air Ne, Kr and Xe observations. *Earth Planet. Sci. Lett.* 244 (1–2), 474–500. <https://doi.org/10.1016/j.epsl.2006.01.032>.
- Tyroller, L., Brennwald, M.S., Mächler, L., Livingstone, D.M., Kipfer, R., 2014. Fractionation of Ne and Ar isotopes by molecular diffusion in water. *Geochim. Cosmochim. Acta* 136, 60–66. <https://doi.org/10.1016/j.gca.2014.03.040>.
- Tyroller, L., Brennwald, M.S., Busemann, H., Maden, C., Baur, H., Kipfer, R., 2018. Negligible fractionation of Kr and Xe isotopes by molecular diffusion in water. *Earth Planet. Sci. Lett.* 492, 73–78.
- Wagner, W., Pruss, A., 1993. International Equations for the Saturation Properties of Ordinary Water Substance. Revised According to the International Temperature Scale of 1990. Addendum to *J. Phys. Chem. Ref. Data* 16, 893 (1987). *J. Phys. Chem. Ref. Data* 22 (3), 783–787. <https://doi.org/10.1063/1.555926>.
- Wang, S., et al., 2021. Characteristics of hydrogen and oxygen isotopes and noble gas isotopes in groundwater of Weishan, Wudalianchi, Northeast China. *Acta Geol Sin Engl.* <https://doi.org/10.1111/1755-6724.14647>.
- Wang, S., Kuang, J., Huang, X., Zhang, H., Zhang, M., Qi, S., Han, Y., Xiao, Z., Wang, S., Tang, L., 2022. Upwelling of Mantle Derived Material in Southeast China: Evidence from Noble Gas Isotopes. *Acta Geol Sin Engl* 96 (1), 100–110.
- Warrier, R.B., Castro, M.C., Hall, C.M., Lohmann, K.C., 2013. Large atmospheric noble gas excesses in a shallow aquifer in the Michigan Basin as indicators of a past mantle thermal event. *Earth Planet. Sci. Lett.* 375, 372–382. <https://doi.org/10.1016/j.epsl.2013.06.001>.
- Wei, W., Hammond, J.O.S., Zhao, D., Xu, J., Liu, Q., Gu, Y., 2019. Seismic evidence for a mantle transition zone origin of the Wudalianchi and Halaha volcanoes in Northeast China. *Geochim. Geophys. Geosyst.* 20 (1), 398–416.
- Wen, T., Castro, M.C., Nicot, J.-P., Hall, C.M., Larson, T., Mickler, P., Darvari, R., 2016. Methane sources and migration mechanisms in shallow groundwaters in Parker and Hood counties, Texas-A Heavy Noble gas analysis. *Environ. Sci. Technol.* 50 (21), 1202–12021.
- Wen, T., Castro, M.C., Nicot, J.-P., Hall, C.M., Pinti, D.L., Mickler, P., Darvari, R., Larson, T., 2017. Characterizing the noble gas isotopic composition of the Barnett shale and strawn group and constraining the source of stray gas in the Trinity aquifer, North-Central Texas. *Environ. Sci. Technol.* 51 (11), 6533–6541.
- Wen, T., Pinti, D.L., Castro, M.C., López-Hernández, A., Hall, C.M., Shouakar-Stash, O., Sandoval-Medina, F., 2018. A noble gas and 87Sr/86Sr study in fluids of the Los Azufres geothermal field, Mexico – Assessing impact of exploitation and constraining heat sources. *Chem. Geol.* 483, 426–441.
- Xu, S., Zheng, G., Nakai, S., Wakita, H., Wang, X., Guo, Z., 2013. Hydrothermal He and CO₂ at Wudalianchi intra-plate volcano, NE China. *J. Asian Earth Sci.* 62, 526–530.
- Zhang, M., Guo, Z., Liu, J., Liu, G., Zhang, L., Lei, M., Zhao, W., Ma, L., Sepe, V., Ventura, G., 2018. The intraplate Changbaishan volcanic field (China/North Korea): A review on eruptive history, magma genesis, geodynamic significance, recent dynamics and potential hazards. *Earth Sci. Rev.* 187, 19–52.
- Zhao, D., 2007. Seismic images under 60 hotspots: Search for mantle plumes. *Gondwana Res.* 12 (4), 335–355. <https://doi.org/10.1016/j.gr.2007.03.001>.
- Zhao, D., 2021. Seismic imaging of Northwest Pacific and East Asia: New insight into volcanism, seismogenesis and geodynamics. *Earth Sci. Rev.* 214, 103507.
- Zhao, W., Guo, Z., Lei, M., Zhang, M., Ma, L., Fortin, D., Zheng, G., 2019. Volcanogenic CO₂ degassing in the Songliao continental rift system, NE China. *Geofluids* 2019, 1–14.
- Zhou, Z., Ballantine, C.J., Kipfer, R., Schoell, M., Thibodeaux, S., 2005. Noble gas tracing of groundwater/coalbed methane interaction in the San Juan Basin, USA. *Geochim. Cosmochim. Acta* 69 (23), 5413–5428. <https://doi.org/10.1016/j.gca.2005.06.027>.